Chapter 2
Mapping Regulatory Interactions of the RNA-Binding Protein LIN28B

2.1 PAR-CLIP Reproducibly Identifies Thousands of Human RNAs Directly Bound by LIN28B

To identify LIN28B binding sites at high resolution, we applied photoactivatable-ribonucleoside-enhanced crosslinking and immunoprecipitation (PAR-CLIP) in combination with next-generation sequencing (Hafner et al. 2010). In PAR-CLIP experiments, nascent RNA is metabolically labeled with the photoreactive ribonucleosides 4-thiouridine (4SU) or 6-thioguanosine (6SG). Crosslinking of protein to 4SU or 6SG-labeled RNA leads to specific T to C or G to A transitions that occur at high-frequency in cDNA sequence reads and mark the protein crosslinking site on the target RNA (Hafner et al. 2010). Briefly, HEK293 cells stably expressing inducible FLAG/HA-tagged LIN28B at physiological levels (see Graf et al. 2013, Supplementary Figure S1 A) were crosslinked after metabolic labeling of RNA with photoreactive ribonucleosides. Immunopurified, ribonuclease treated and radiolabeled LIN28B-RNA complexes were separated by SDS-PAGE and bands migrating at the expected molecular weight of LIN28B protein were excised (Fig. 2.1a, also see Graf et al. 2013, Supplementary Figure S1 B). Protein-protected RNA fragments were recovered and converted into a cDNA library amenable to Illumina sequencing.

In total we performed three independent PAR-CLIP experiments (two biological replicates with 4SU and one experiment with 6SG; see Graf et al. 2013, Supplementary Figure S1 C and Supplementary Table S1). Sequence reads were aligned to the spliced human transcriptome and overlapping reads were used to build sequence read clusters. In PAR-CLIP experiments using 4SU, diagnostic T-C mutations were

---

Results presented in this chapter were originally published in the journal article: "Identification of LIN28B-bound mRNAs reveals features of target recognition and regulation. RNA Biology *10*, 1146-1159". This article can be accessed at:

http://dx.doi.org/10.4161/rna.25194

M. Munschauer, *High-Resolution Profiling of Protein-RNA Interactions*,
Springer Theses, DOI 10.1007/978-3-319-16253-9_2

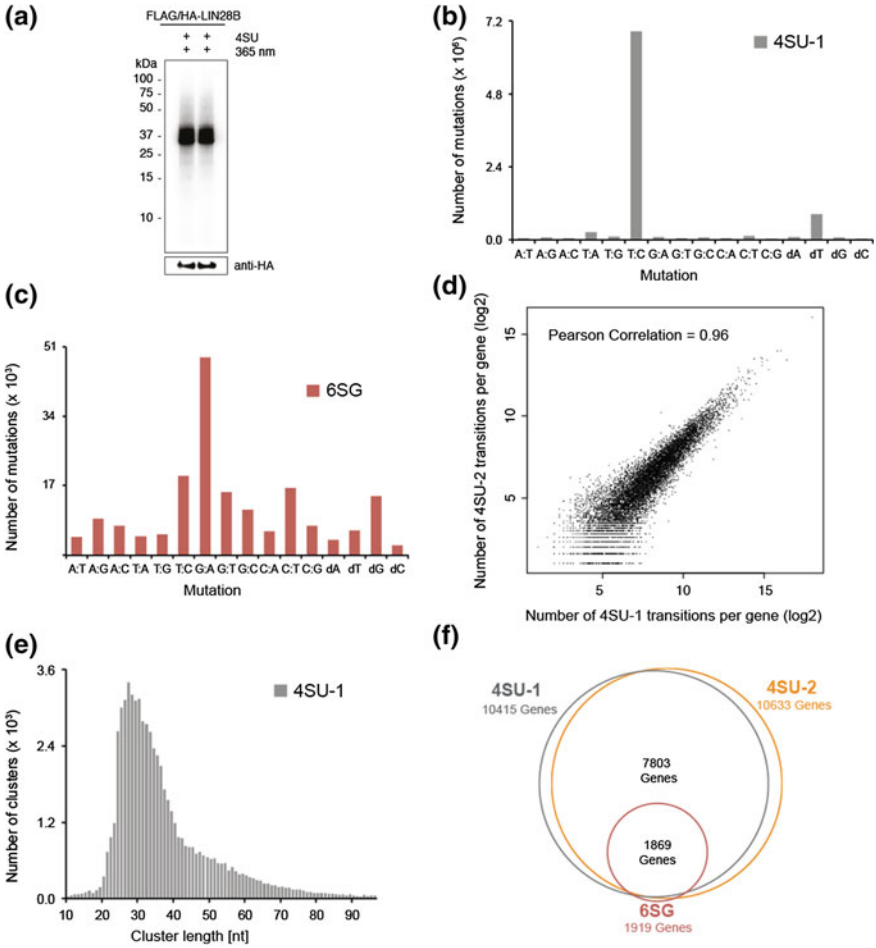

Fig. 2.1 PAR-CLIP reproducibly identifies thousands of human mRNAs directly bound by LIN28B. **a** Autoradiogram of SDS-PAGE gel, transferred to a nitrocellulose membrane. Crosslinked protein-RNA complexes migrating at 39 kDa correspond to epitope-tagged LIN28B. Anti-HA Western blot validates immunoprecipitation of FLAG/HA-LIN28B. Lanes 1 and 2 show protein-RNA complexes used for generation of 4SU-1 and 4SU-2 PAR-CLIP libraries. **b** and **c** Frequency of nucleotide mutations detected in 4SU-1 and 6SG PAR-CLIP libraries after alignment to spliced human transcriptome. dA, dT, dG and dG indicate respective nucleotide deletions. **d** Number of diagnostic transitions per gene observed in 4SU-1 and 4SU-2 experiments. dA, dT, dG and dG indicate respective nucleotide deletions. **e** Length distribution of 4SU-1 PAR-CLIP sequence clusters after quality filtering. **f** Scaled Venn diagram of target genes with at least two independent diagnostic transitions in indicated PAR-CLIP libraries

30-fold more abundant than any other mutation within clustered sequence reads (Fig. 2.1b, also see Graf et al. 2013, Supplementary Figure S1 D). Similarly, but less pronounced, the diagnostic G-A mutation was the most abundant mutation

observed in sequence clusters derived from 6SG PAR-CLIP experiments (Fig. 2.1c). In addition to these diagnostic mutations and consistent with previous reports (Kishore et al. 2011; Lebedeva et al. 2011; Zhang and Darnell 2011), we observed respective T or G deletions at crosslinking sites, however less frequently (compare Fig. 2.1b, c). We therefore considered the respective nucleotide transitions as well as nucleotide deletions as indicators for direct protein-RNA crosslinking events and refer to them as diagnostic transitions in what follows.

When comparing the number of diagnostic transitions per gene in the two 4SU experiments, we observed a high reproducibility between biological replicates (Pearson Correlation: 0.96) (Fig. 2.1d). Furthermore, crosslinking positions in one 4SU library were highly reproducible in the other 4SU replicate library (see Graf et al. 2013, Supplementary Figure S1 E and S1 F). Comparing mRNA expression levels of genes covered by the top 1000 4SU PAR-CLIP binding sites to those of all transcribed genes indicated a good dynamic detection range (see Graf et al. 2013, Supplementary Figure S1 G). Figure 2.1e shows that the cluster length distribution peaked at a cluster length of $\sim$27 nucleotides.

The total number of target genes identified in each PAR-CLIP experiment was strongly dependent on the photoreactive ribonucleosides used, likely reflecting different crosslinking efficacies (Hafner et al. 2010). While the two 4SU experiments identified target transcripts of 10,415 and 10,633 genes, respectively, only 1919 genes were detected in the 6SG PAR-CLIP. Despite obvious differences in the total number of target transcripts captured in 4SU or 6SG experiments, the identity of target genes was largely overlapping (Fig. 2.1f). The surprisingly large number of bound transcripts detected in both 4SU experiments points towards an unusual widespread mode of LIN28B target interaction that encloses the majority of all expressed transcripts. A similar observation was recently described for LIN28A (Cho et al. 2012).

2.2 LIN28B Binds to *Let-7* Precursors and Protein Coding Transcripts

For further analysis, we defined a conservative set of sequence clusters that showed at least two independent diagnostic transitions in overlapping reads from 4SU and 6SG PAR-CLIP libraries. Applying these criteria with a flank of 30 nucleotides, we retained 2540 conservative sequence clusters mapping to transcripts of 1527 protein-coding genes. Almost all of LIN28B binding sites were detected within 3′ UTRs (51 %) and CDS (44 %) of mRNAs (Fig. 2.2b). While early studies on the mRNA binding activity of LIN28 focused on binding elements in 3′ UTRs (Peng et al. 2011; Polesskaya et al. 2007; Xu et al. 2009), the high frequency of CDS targeting is surprising, but not unreported for other RNA-binding proteins (Baltz et al. 2012).

Consistent with previous in vitro experiments, we found pre-let-7b and pre-let-7f to be directly contacted by LIN28B in loop and hairpin regions in all 3 PAR-CLIP

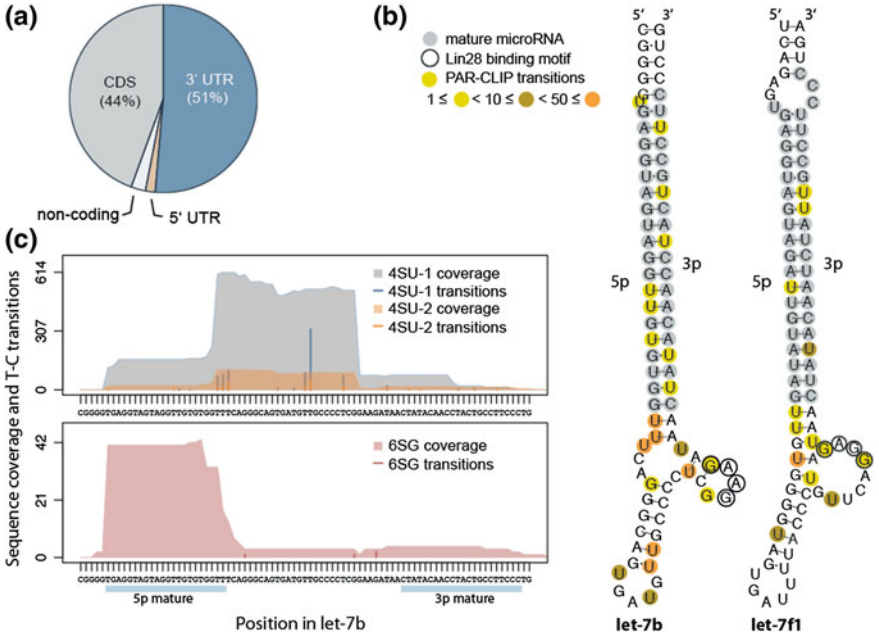

Fig. 2.2 LIN28B binds to 3′ UTRs and CDS of protein coding genes and interacts with let-7 precursors. **a** Distribution of LIN28B-binding sites in conservative sequence clusters to non-coding RNAs and different transcript regions (5′ UTR, CDS and 3′ UTR) of protein-coding genes. **b** Identified LIN28B binding sites in let-7b and let-7f1 precursors. Mature microRNA sequences (*light-gray*), biochemically identified GGAG motif (*encircled*) and weighted PAR-CLIP transition sites (*yellow* to *orange*) are indicated. Structures are adapted from RNAfold outputs (ViennaRNA). **c** Alignment of sequence coverage signal and diagnostic nucleotide transitions observed in 4SU-1 (*gray*), 4SU-2 (*orange*) and 6SG (*red*) libraries to the genomic region encoding let-7b precursor

experiments, while pre-let-7d was detected in 4SU experiments only (Fig. 2.2b, also see C, Graf et al. 2013, Supplementary Figures S2 A and B). Since the let-7 family of miRNAs represents the best-studied group of functionally regulated LIN28 targets, we considered them as important internal controls. Diagnostic transitions within the loop regions of pre-let-7b and pre-let-7f precisely occurred in the previously described GGAG binding motif (Fig. 2.2b, c), thus validating that our approach captures functional LIN28B target interactions at high resolution. Interestingly, Fig. 2.2c shows extensive sequence coverage of 4SU experiments in the pre-let-7b loop region, while 6SG preferentially captured the 5p stem region of the same precursor. Apart from the let-7 family we found only 3 other miRNA precursors (pre-miR-19b-1, pre-miR-663, and pre-miR-16-2) being bound by LIN28B, underlining the specificity of our approach (see Graf et al. 2013, Supplementary Figure S2 C).

2.3 Target Transcripts Are Enriched for a RGGSWG Consensus Motif

To enable identification of sequence motifs responsible for LIN28B mRNA binding, we generated crosslink centered regions (30 nucleotides upstream and downstream of crosslinking sites) from the conservative set of sequence clusters. We applied MEME motif finding algorithm (Bailey et al. 2009) on the top 300 conservative 6SG-centered target regions in 3′ UTRs and identified RGGSWG (R = G or A, S = G or C, W = A or T) as the most enriched motif (E = 0.14, 74 sites) (Fig. 2.3a). Consistently, GGAG was the most frequently observed tetramer in all 6SG-centered binding sites within our set of conservative target transcripts (Fig. 2.3b). Reducing the window size from 60 to 10

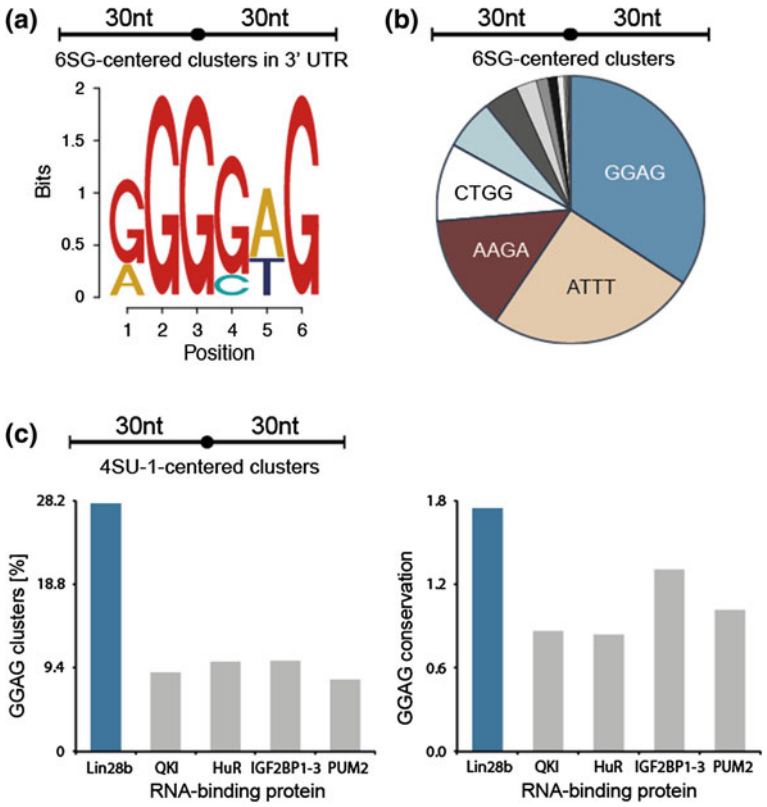

Fig. 2.3 LIN28B target transcripts are enriched for GGAG consensus motif. **a** Top sequence motif identified by MEME in top 300 6SG centered 3′ UTR binding sites (extended by 30 nucleotides upstream and downstream) within conservative sequence clusters. **b** Most frequent tetramers within 6SG centered conservative clusters, extended by 30 nucleotides upstream and downstream of 6SG-crosslinks. **c** Frequency of GGAG in the top 1000 sequence clusters from indicated PAR-CLIP data sets (*left*) and mean vertebrate conservation (phyloP) of GGAG within those sequence clusters (*right*)

nucleotides around crosslinked sites left the results largely unchanged, indicating that the GGAG motif is mostly observed in the vicinity of 6SG crosslinks (see Graf et al. 2013, Supplementary Figure S3 A). On the other hand, when applying our analysis to random G-centered sequences derived from the same transcript set, AGAA was the most frequently observed tetramer (see Graf et al. 2013, Supplementary Figure S3 B). Interestingly, a motif search in CDS clusters yielded AAGRWG (R = A or G), which is highly similar to the LIN28A consensus sequence reported by Cho et al. 2012 (also see Graf et al. 2013, Supplementary Figure S3 C). To exclude that a technical bias leads to an enrichment of GGAG in our PAR-CLIP data, we compared the occurrence of the GGAG motif in LIN28B PAR-CLIP clusters to the presence of the same motif in PAR-CLIP data from previously studied RBPs. Figure 2.3c shows that GGAG containing clusters were at least twofold more enriched in LIN28B PAR-CLIP data. At the same time, the evolutionary conservation of the GGAG motif in LIN28B clusters exceeded the conservation in other PAR-CLIP clusters by a factor of 2 (Fig. 2.3 C, also see Graf et al. 2013, Supplementary Figure S3 D). In conclusion, the GGAG motif appears to be a crucial determinant for LIN28B binding, not only in let-7 precursor interaction, but also in recognition of target mRNAs. While co-crystals of LIN28 and let-7 revealed that GGAG is contacted by the ZKD of LIN28, evidence for a distinct binding motif or region contacted by the CSD is less clear. Nam et al. proposed NGNGAYNNN within a closed loop as a consensus for CSD binding, whereas Mayr et al. identified a GUNNUNN motif (Mayr et al. 2012; Nam et al. 2011). However, neither of these motifs is enriched in our dataset.

2.4 Individual Domain PAR-CLIP Enables Characterization of Domain Specific Target Interactions

To further explore the contribution of CSD and ZKD binding to LIN28 target recognition, we generated a stable cell line, expressing FLAG/HA-LIN28B-HIS protein that contains a PreScission protease cleavage site between the two RNA binding domains at amino acids 108–114 (Fig. 2.4a). Following crosslinking and RNase digest, the N-terminal FLAG-tag was used to immunopurify the full length protein. We then used PreScission protease to cleave crosslinked LIN28B protein between CSD and ZKD. Following cleavage of full length LIN28B, the C-terminal HIS-tag enabled purification of the ZKD fragment allowing us to perform individual domain PAR-CLIP (iDo-PAR-CLIP). Resulting domain fragments were separated on SDS-PAGE (Fig. 2.4b), and excised from the gel. Crosslinked RNA fragments were converted into a cDNA library amenable for Illumina sequencing. After aligning the sequence reads to the spliced human transcriptome, we detected characteristic PAR-CLIP nucleotide transitions (see Graf et al. 2013, Supplementary Figures S4 A and B). Surprisingly, we observed differences in CSD and ZKD crosslinking patterns on individual target transcripts. Figure 2.4 C exemplifies

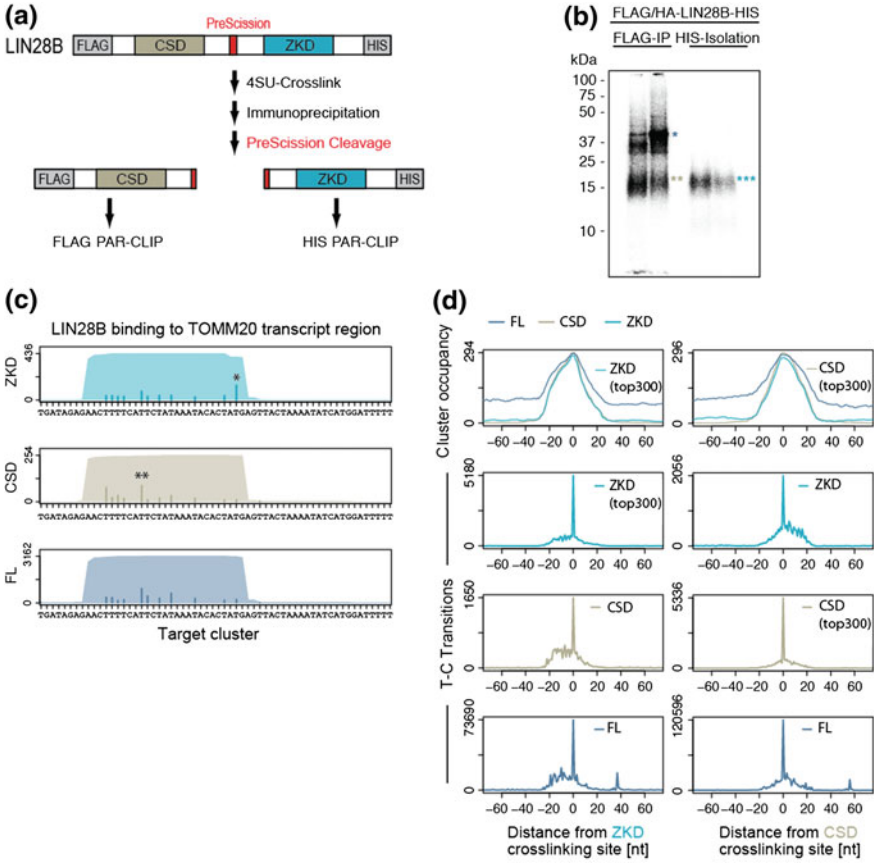

Fig. 2.4 iDo-PAR-CLIP (individual domain PAR-CLIP) enables characterization of domain specific target interactions. **a** Domain structure of FLAG/HA-LIN28B-HIS protein harboring a PreScission protease cleavage site that replaces amino acids 108-114 in LIN28B. Schematic representation of iDo-PAR-CLIP approach. **b** Autoradiogram of SDS-PAGE gel, transferred to a nitrocellulose membrane. Crosslinked protein-RNA complex migrating at 39 kDa (*blue single asterisk*) corresponds to full length LIN28B protein. Two beige asterisks indicate N-terminally FLAG/HA-tagged LIN28B CSD fragment after PreScission protease cleavage. Three cyan asterisks indicate C-terminally HIS-tagged LIN28B ZKD fragment. **c** Full-length LIN28B and individual domain binding sites in TOMM20 transcript region. Sequence coverage and number of crosslinks derived from 4SU PAR-CLIPs of ZKD, CSD, and LIN28B full-length (FL) protein are shown. *Asterisks* indicate preferred local crosslinking site. **d** Global analysis of CSD and ZKD crosslinking patterns in iDo-PAR-CLIP data. *Top panel* comparison of cluster occupancy (number of cluster at respective position). *Lower panels* diagnostic transitions observed in CSD, ZKD, and FL PAR-CLIP clusters. *Left column* crosslinking signal in ZKD, CSD, and FL PAR-CLIPs, centered on strongest local crosslinking site in ZKD iDo-PAR-CLIP data. *Right column* crosslinking signal in ZKD, CSD, and full-length PAR-CLIPs, centered on preferred crosslinking site in CSD iDo-PAR- CLIP data

LIN28B domain interactions on TOMM20 mRNAs. A global analysis revealed that both domains bound to largely overlapping regions with highly similar cluster occupancy profiles (determined as the number of clusters mapping to the respective region) (Fig. 2.4d, top panel). However, centering sequence clusters on the strongest local transition sites observed in the ZKD PAR-CLIP showed increased CSD crosslinking in a 5′-proximal region of ZKD binding sites (Fig. 2.4d, left column). Consistently, elevated ZKD crosslinking was observed 3′ of CSD binding sites (Fig. 2.4d, right column). Comparing the number of diagnostic transitions observed 5′ and 3′ of the respective preferred crosslinking site, we found highly significant differences in CSD and ZKD crosslinking patterns (ZKD $p = 4.7 \times 10^{-15}$; CSD $p = 4.9 \times 10^{-06}$) (Fig. 2.4d). Together these results indicate that both RNA binding domains interact with the same RNA region and bind in close proximity of each other, suggesting a defined 5′–3′ domain orientation of LIN28B CSD and ZKD on target RNAs.

Next we used the full length LIN28B 4SU PAR-CLIP library to overlap the top 300 CSD or ZKD binding sites and deduce RNA binding motifs that might be specific to CSD or ZKD target interactions. We found DGGGAG (D = A, T, or G) to be the best scoring motif in the top 300 ZKD-overlapping 4SU binding sites. Conversely, the best scoring motif observed in the top 300 CSD-overlapping 4SU binding sites was UUUUCC and rather distinct from the top scoring ZKD motif. Although we detect the domain-specific motifs with low frequency, our findings are consistent with biochemical efforts, elucidating LIN28B binding preferences on let-7 precursors (Desjardins et al. 2012; Lei et al. 2012; Loughlin et al. 2012; Mayr et al. 2012; Nam et al. 2011).

2.5 LIN28B Enhances Protein Production of mRNA Target Transcripts

To examine the effect LIN28B exerts on expression of its mRNA target transcripts, we performed pulsed SILAC proteomics measurements upon LIN28B knock down. Pulsed stable isotope labeling by amino acids in cell culture (pSILAC) was essentially carried out as described before (Lebedeva et al. 2011; Selbach et al. 2008) (Schwanhäusser et al. 2009). Briefly, cells were grown in medium supplemented with ‘light’ stable isotope labeled amino acids. Upon knockdown of endogenous LIN28B, siRNA transfected cells were cultured for 24 h in medium containing ‘medium-heavy’ stable isotope labeled amino acids, while mock treated cells were grown in medium containing ‘heavy’ stable isotope labeled amino acids (see Graf et al. 2013, Supplementary Fig. 1c). The labeled amino acids are incorporated into newly synthesized proteins, leading to a mass shift of proteins derived from LIN28B knock down (‘medium-heavy’) and mock treated (‘heavy’) cells, allowing the quantification of changes in newly synthesized protein levels independent of the pool of ‘light’ labeled pre-existing proteins. We used two different

siRNAs in independent experiments and achieved 80–90 % decrease in LIN28B mRNA levels, resulting in a significant reduction of LIN28B protein level (see Graf et al. 2013, Supplementary Figure S5 A). In measurements of two biological replicates (Pearson Correlation = 0.71; see Graf et al. 2013, Supplementary Figure S5 B) we were able to quantify changes in protein synthesis for about 4500 proteins. Interestingly, mRNA transcripts bound by LIN28B showed significantly higher protein expression levels in mock treated cells when compared to LIN28B knock down cells ($p < 0.003$) (Fig. 2.5a, also see Graf et al. 2013, Supplementary Figure S5 C). Next, we subdivided the mRNA targets into different groups based on the location of LIN28B binding sites and found that targets bound within the CDS showed a mild, but significantly higher change in protein synthesis when compared

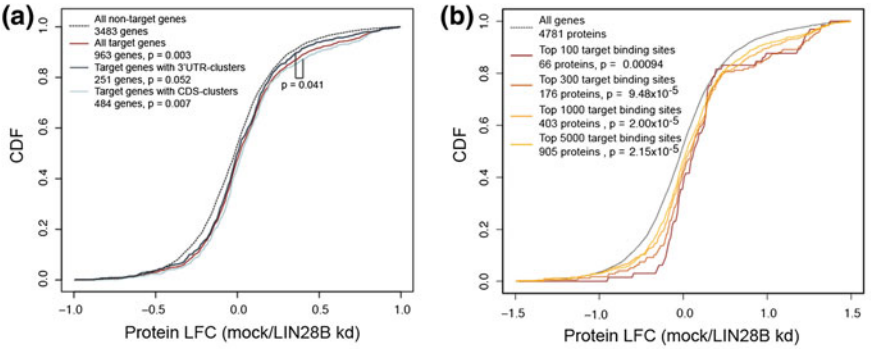

(c)

- - + siRNA 2
- + - siRNA 3

anti-LIN28B
anti-TARDP
anti-HNRNPK
anti-RPL7
anti-UPF1
anti-VCL

Gene symbol	PAR-CLIP score (6SG)	pSILAC LFC (mock/kd) siRNA2, rep. 1	pSILAC LFC (mock/kd) siRNA2, rep. 2	pSILAC LFC (mock/kd) siRNA3
LIN28B	52	1.946131952	nan	nan
TARDBP	2	0.288181352	0.527051942	0.425973472
HNRNPK	26	0.081339627	0.44955461	0.470692435
RPL7	20	0.821383684	0.586464208	0.59086378

Fig. 2.5 LIN28B globally enhances protein synthesis of target mRNAs. **a** Cumulative distribution of log2 transformed changes in newly synthesized protein levels, measured by pulsed SILAC upon LIN28B knock down (pSILAC data using siRNA2, replicate 1 is shown). PAR-CLIP targets with 3′ UTR binding sites only and targets with CDS binding sites are compared to all targets and non-targets. **b** Cumulative distribution of log2 transformed changes in newly synthesized protein levels upon LIN28B knock down. Genes covered by the top 5000, 1000, 300 and 100 conservative binding sites are shown (pSILAC data from siRNA2, replicate 1 is shown). All indicated P-values are based on Wilcoxon rank sum test. **c** Western analysis of target transcript encoded proteins upon LIN28B knockdown using siRNA2 and siRNA3. UPF1 and vinculin (VCL) served as controls. Table indicates log2 fold changes in protein synthesis upon LIN28 knockdown as determined by pSILAC experiments. *CDF* cumulative distribution function, *LFC* log2 fold change

to 3′ UTR bound targets ($p < 0.041$) (Fig. 2.5a, also see Graf et al. 2013, Supplementary Figure S5 C). Interestingly, we observed increasing changes in protein synthesis when considering only the top 5000, 1000, 300 or 100 binding sites in our conservative set of target clusters (Fig. 2.5b, also see Graf et al. 2013, Supplementary Figure S5 D). This observation was confirmed for the group of genes mapping to the top 100 binding sites in 4SU and 6SG PAR-CLIP experiments (see Graf et al. 2013, Supplementary Figure S5 E). We next focused on the 100 lowest ranked binding sites in 4SU and 6SG PAR-CLIPs and did not observe significant changes in protein synthesis for the corresponding genes (see Graf et al. 2013, Supplementary Figure S5 F). Thus, we hypothesize that protein production from highly ranked PAR-CLIP targets is more likely to be regulated by LIN28B. This effect is independent of let-7, as PicTar (Anders et al. 2012; Krek et al. 2005) predicted let-7 targets, as a group, do not show a significant change in protein production upon LIN28 knock down (see Graf et al. 2013, Supplementary Figure S5 G). The observation that CDS bound targets show enhanced protein production when compared to 3′ UTR bound targets suggests a previously unappreciated aspect of LIN28B regulation and points towards a functional relevance of LIN28B binding events in the CDS. We validated the changes in protein synthesis as observed in pSILAC experiments in LIN28B knockdown cells by Western analysis of target transcript encoded proteins (Fig. 2.5c). A reduction in protein levels was observed for the LIN28-targets TARDBP, HNRNPK, and RPL7 upon LIN28 depletion, whereas no significant protein changes could be detected for non-targets UPF1 and vinculin (VCL).

2.6 LIN28B Controls Core Cell Cycle Regulators

Gene Ontology enrichment analysis of LIN28B targeted transcripts revealed a highly significant enrichment of genes involved in ribosome ($p = 3.0 \times 10^{-120}$), cell cycle ($p = 1.3 \times 10^{-36}$), spliceosome ($p = 4.0 \times 10^{-36}$), and pathways in cancer ($p = 6.7 \times 10^{-30}$) (see Graf et al. 2013, Supplementary Table S3). Importantly, genes belonging to the most significantly enriched GO-term "ribosome" also represent the strongest LIN28B PAR-CLIP targets and exhibit highest log2 fold changes in pSILAC experiments upon LIN28B knock down (see Graf et al. 2013, Supplementary Table S2 and Supplementary Figure S6). LIN28B binding and regulation of mRNA targets involved in cell cycle control and gene regulation is consistent with its well established role in stem cell differentiation and oncogenesis (Thornton and Gregory 2012). In agreement with these findings we observed a strong reduction of cell proliferation in LIN28B knockdown cells (Fig. 2.6a). Accordingly, cell cycle analysis by DNA content (propidium iodide staining) revealed a substantially higher percentage of cells residing in the G2/M phase under LIN28B knock down conditions (Fig. 2.6b), further supporting the importance of LIN28B-mRNA interactions in cell cycle control.

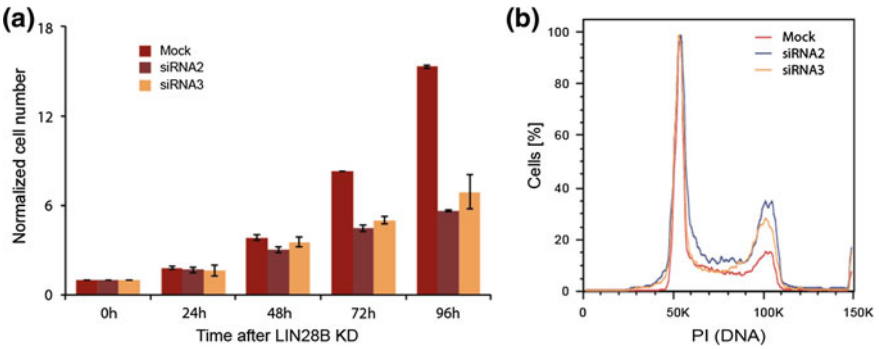

Fig. 2.6 LIN28B controls cell growth and regulates the cell cycle. **a** Normalized cell numbers following LIN28B knock down using two different siRNAs over a period of 96 h. **b** Flow cytometry plot of cell cycle staining by propidium iodide after 72 h of LIN28B knock down. Results are representative for three independent experiments using two different siRNAs

References

Anders G, Mackowiak SD, Jens M, Maaskola J, Kuntzagk A, Rajewsky N, Landthaler M, Dieterich C (2012) doRiNA: a database of RNA interactions in post-transcriptional regulation. Nucleic Acids Res 40:D180–D186

Bailey TL, Boden M, Buske FA, Frith M, Grant CE, Clementi L, Ren J, Li WW, Noble WS (2009) MEME SUITE: tools for motif discovery and searching. Nucleic Acids Res 37:W202–W208

Baltz AG, Munschauer M, Schwanhäusser B, Vasile A, Murakawa Y, Schueler M, Youngs N, Penfold-Brown D, Drew K, Milek M et al (2012) The mRNAbound proteome and its global occupancy profile on protein-coding transcripts. Mol Cell 46:674–690

Cho J, Chang H, Kwon SC, Kim B, Kim Y, Choe J, Ha M, Kim YK, Kim VN (2012) LIN28A is a suppressor of ER-associated translation in embryonic stem cells. Cell 151:765–777

Desjardins A, Yang A, Bouvette J, Omichinski JG, Legault P (2012) Importance of the NCp7-like domain in the recognition of pre-let-7 g by the pluripotency factor Lin28. Nucleic Acids Res 40:1767–1777

Graf R, Munschauer M, Mastrobuoni G, Mayr F, Heinemann U, Kempa S, Rajewsky N, Landthaler M (2013) Identification of LIN28B-bound mRNAs reveals features of target recognition and regulation. RNA Biol 10:1146–1159

Hafner M, Landthaler M, Burger L, Khorshid M, Hausser J, Berninger P, Rothballer A, Ascano M Jr, Jungkamp A-C, Munschauer M et al (2010) Transcriptome-wide identification of RNA-binding protein and MicroRNA target sites by PAR-CLIP. Cell 141:129–141

Kishore S, Jaskiewicz L, Burger L, Hausser J, Khorshid M, Zavolan M (2011) A quantitative analysis of CLIP methods for identifying binding sites of RNA-binding proteins. Nat Methods 8:559–564

Krek A, Grün D, Poy MN, Wolf R, Rosenberg L, Epstein EJ, MacMenamin P, da Piedade I, Gunsalus KC, Stoffel M et al (2005) Combinatorial microRNA target predictions. Nat Genet 37:495–500

Lebedeva S, Jens M, Theil K, Schwanhäusser B, Selbach M, Landthaler M, Rajewsky N (2011) transcriptome-wide analysis of regulatory interactions of the RNA-binding protein HuR. Mol Cell 43:340–352

Lei XX, Xu J, Ma W, Qiao C, Newman MA, Hammond SM, Huang Y (2012) Determinants of mRNA recognition and translation regulation by Lin28. Nucleic Acids Res 40:3574–3584

Loughlin FE, Gebert LFR, Towbin H, Brunschweiger A, Hall J, Allain FH-T (2012) Structural basis of pre-let-7 miRNA recognition by the zinc knuckles of pluripotency factor Lin28. Nat Struct Mol Biol 19:84–89

Mayr F, Schütz A, Döge N, Heinemann U (2012) The Lin28 cold-shock domain remodels pre-let-7 microRNA. Nucleic Acids Res 40:7492–7506

Nam Y, Chen C, Gregory RI, Chou JJ, Sliz P (2011) Molecular basis for interaction of let-7 microRNAs with Lin28. Cell 147:1080–1091

Peng S, Chen L-L, Lei X-X, Yang L, Lin H, Carmichael GG, Huang Y (2011) Genome-wide studies reveal that Lin28 enhances the translation of genes important for growth and survival of human embryonic stem cells. Stem Cells 29:496–504

Polesskaya A, Cuvellier S, Naguibneva I, Duquet A, Moss EG, Harel-Bellan A (2007) Lin-28 binds IGF-2 mRNA and participates in skeletal myogenesis by increasing translation efficiency. Genes Dev 21:1125–1138

Schwanhäusser B, Gossen M, Dittmar G, Selbach M (2009) Global analysis of cellular protein translation by pulsed SILAC. Proteomics 9:205–209

Selbach M, Schwanhäusser B, Thierfelder N, Fang Z, Khanin R, Rajewsky N (2008) Widespread changes in protein synthesis induced by microRNAs. Nature 455:58–63

Thornton JE, Gregory RI (2012) How does Lin28 let-7 control development and disease? Trends Cell Biol 1–9

Xu B, Huang Y (2009) Histone H2a mRNA interacts with Lin28 and contains a Lin28-dependent posttranscriptional regulatory element. Nucleic Acids Res 37:4256–4263

Zhang C, Darnell RB (2011) Mapping in vivo protein-RNA interactions at single-nucleotide resolution from HITS-CLIP data. Nat Biotechnol 29:607–614

http://www.springer.com/978-3-319-16252-2

High-Resolution Profiling of Protein-RNA Interactions

Munschauer, M.

2015, XXIII, 121 p. 25 illus., 20 illus. in color., Hardcover
ISBN: 978-3-319-16252-2